Available online at www.sciencedirect.com
ScienceDirect
Planetary and Space Science 56 (2008) 901–912
Planetary and Space Science
www.elsevier.com/locate/pss

Derivation of density and temperature from the Cassini–Huygens CAPS electron spectrometer

G.R. Lewis[a,*], N. André[b], C.S. Arridge[a], A.J. Coates[a], L.K. Gilbert[a], D.R. Linder[a], A.M. Rymer[c]

[a]*Mullard Space Science Laboratory, University College London, UK*
[b]*Research and Science Support Department, European Space Agency, Noordwijk, The Netherlands*
[c]*Applied Physics Laboratory, Johns Hopkins University, Laurel, MD, USA*

Received 20 February 2007; received in revised form 7 December 2007; accepted 17 December 2007
Available online 25 January 2008

Abstract

In this paper we present two methods to derive electron fluid parameters from the CAPS–ELS spectrometer on board the Cassini spacecraft currently in orbit around Saturn. In the first part of the paper we give a basic overview of the instrument and describe the challenges inherent in the derivation of density and temperature values using these techniques. We then describe a method to calculate electron moments by integrating the particle distribution function. We also describe a second technique in which we fit the electron energy spectrum with a Gaussian curve and use the peak energy of this curve to derive density and temperature values. We then compare the two methods with particular emphasis on their application to Cassini SOI observations in the saturnian environment and point out the limitations of the two techniques. We will show that results from the two very different methods are in agreement when the physical properties of the environment and of the observed electron populations have been inferred from inspection of the raw data. Finally we will suggest future developments that will remove these limitations.

Keywords: Electron; Density; Temperature; Cassini; Saturn

1. Introduction

During the four years following Cassini–Huygens' successful insertion into orbit around Saturn on 1 July 2004, the planet's space environment is being studied in detail. The instrumental suite carried on board the spacecraft offers a unique opportunity to explore, in-depth, the plasma and fields environment of the planet, previously described with the help of the limited fly-by data returned by Pioneer 11 and by the Voyager 1 and 2 spacecraft more than 20 years ago. The magnetospheric and plasma science instruments are enabling us to detail the physical and chemical processes taking place in the different regions of this complex environment, in strong interaction with all components of the planetary system: the planet itself, the rings, numerous satellites (the icy moons and Titan), and various dust, neutral, and plasma populations (Blanc et al., 2002). The spacecraft carries an electron spectrometer (ELS) which, together with the ion mass spectrometer (IMS) and the ion beam spectrometer (IBS), collectively make up the Cassini plasma spectrometer (CAPS) (Young et al., 2004). The CAPS–ELS is designed to study the low-energy electron populations observed in situ in Saturn's magnetosphere, from the micro-physical to the global scale (Linder et al., 1998; Young et al., 2004). Such studies require the characterization of the electron velocity distributions and the derivation of various bulk plasma parameters, such as density, temperature, velocity, pressure and possibly higher-order terms. Well-documented methods for obtaining these parameters from space observations have been developed and involve taking integral moments of the distribution about a three dimensional velocity space (Paschmann et al., 1998). These methods however, have been developed for spinning spacecraft where, in one revolution, the entire surrounding space is

*Corresponding author.
E-mail address: grl@mssl.ucl.ac.uk (G.R. Lewis).

0032-0633/$ - see front matter © 2008 Elsevier Ltd. All rights reserved.
doi:10.1016/j.pss.2007.12.017

sampled. Since Cassini–Huygens is a three-axis stabilized spacecraft, this imposes strong constraints on the instrument field of view, with the CAPS–ELS instrument at best only sampling just over half of the available surrounding space. The purpose of this paper is to describe two techniques developed to derive the density and temperature of the surrounding plasma using the electron data as measured by the CAPS–ELS instrument. It will serve as a reference point for the CAPS–ELS data when they enter the public domain. The paper is organised in the following way. In Section 2, we summarize the properties of the instrument and describe the procedure used to correct the instrument's raw data (count rates) for photoelectron contamination using the electron velocity distribution (phase space density). In Section 3, we detail the first technique (the 3d method) based on the traditional integral method with the assumption that the electron distribution function is isotropic. Using this method, the electron density and temperature are obtained by taking the zeroth and second order moments of the velocity distribution function, respectively. In Section 4, we detail the second technique (the 1d method). This relies on the assumption that the velocity distribution function can be approximated by an isotropic Maxwellian. Using this method, the electron density and temperature are obtained by relating the peak energy to these values. In Section 5, we apply these techniques to saturn orbit insertion (SOI) observations and compare their results, discussing their respective advantages and limitations in the study of the different plasma regions identified by Young et al. (2005). In Section 6, we identify future improvements of these techniques and conclude our study. The methods described in the following sections are restricted by the assumption of isotropic electron distributions, and consequently, only a limited part of the information recorded by the CAPS–ELS spectrometer is used to derive electron moments. This assumption produces severe limitations on the data products obtained by the CAPS–ELS. There is scope, however, to make future improvements to the methods described here. This would include the use of measurements obtained by all anodes as well as the motion of the rotating platform in order to derive moments corresponding first to gyrotropic and then to the real electron distributions. Despite these limitations, we will show that the methods detailed here provide useful data products with reasonable level of accuracy.

2. The CAPS–ELS instrument

2.1. The instrument

The CAPS–ELS is a hemispherical top-hat electrostatic analyzer (Young et al., 2004; Linder et al., 1998; Coates et al., 1996). Electrons enter a baffled collimeter structure and undergo electrostatic analysis between two concentric spherical plates. The energy resolution, $\Delta E/E$ for electrons exiting the analyser is 16.7%. The analysed electrons then strike a microchannel plate with a gain of 2×10^6. The electron cloud is then accelerated towards the anode structure which determine the direction of the electron's motion. There are eight anodes each having an angular coverage of 20° by 5° and are orientated in a semi circle about the spacecraft's X-axis, covering 160° by 5°. The CAPS–ELS is mounted on a rotating platform, referred to as the 'actuator'. The actuator can rotate about the spacecraft's Z-axis at a nominal rate of $1^\circ\,s^{-1}$ through a

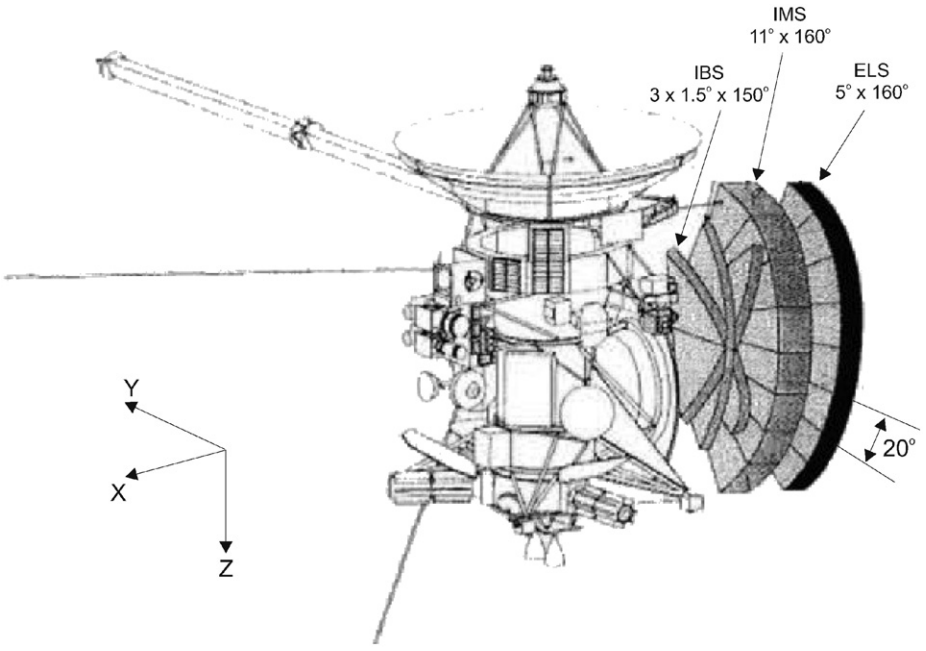

Fig. 1. An illustration to show the layout of the three CAPS instruments on board Cassini together with their relative orientations. The shaded regions are exaggerations of the anode layout in each instrument.

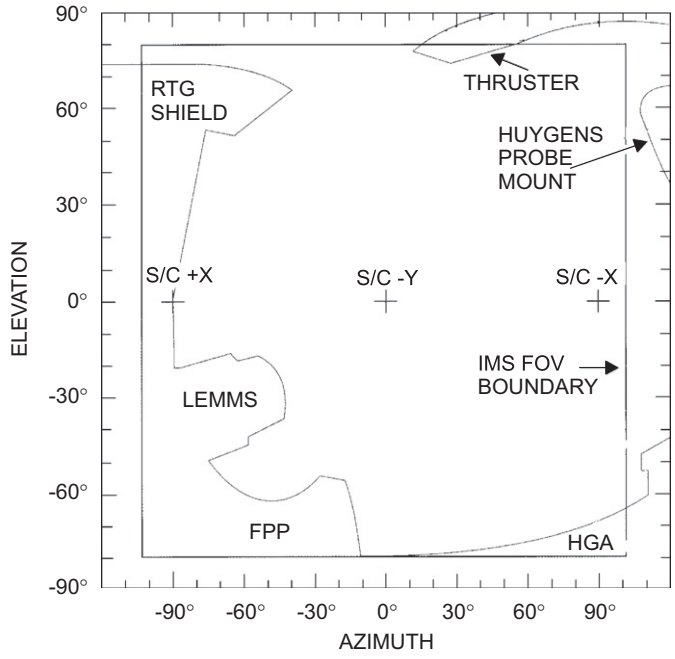

Fig. 2. An illustration of the field of view of the CAPS–IMS instrument on board Cassini. This is identical to the CAPS–ELS as they are mounted beside each other.

range of ±104°. This is illustrated in Fig. 1. The layout of the eight anodes together with the actuator provide a CAPS–ELS coverage of approximately 208° by 160° of the surrounding spherical space. This equates to approximately 56% of the full 4π space. As can be seen in Fig. 1, the CAPS–ELS instrument is mounted on top of the CAPS–IMS instrument and so their fields of view will be essentially identical. The field of view of the CAPS–IMS sensor, and therefore of the CAPS–ELS sensor is illustrated in Fig. 2. During operation the analyzer sweeps through a 64-level energy spectrum ranging from 0.58 to 26,000 eV of the ambient electrons with respect to the spacecraft potential. Apart from the lower few steps, the spectrum is logarithmically spaced to match the intrinsic resolution, $(\Delta E/E)$ of the instrument. The full range of energy values is shown in Table 1. Each of these voltages is held for a period of 31.25 ms. Of this time, 25% is 'dead time' which allows the analyzer voltage to "settle". The remaining 75% is spent accumulating electrons which are returned as count values. The 64th energy level is a "fly-back" step to change the voltage from the lowest to the highest energy. During this time no readings are taken. The analyzer can therefore return 63 values of electron counts in 2 s, for each of the eight anodes.

2.2. Correcting for spacecraft potential and photoelectron contamination

The spacecraft potential is determined by the current balance between positively charged ions and negatively charged electrons, which include ambient, secondary, back scattered, and photoelectrons (Whipple, 1981). When sunlit

Table 1
CAPS–ELS centroid energy values in eV and their corresponding measurement bin numbers

Bin	Energy	Bin	Energy	Bin	Energy	Bin	Energy
1	26,040	17	2112	33	171.7	49	13.98
2	22,227	18	1805	34	146.9	50	11.64
3	18,991	19	1544	35	125.1	51	9.89
4	16,256	20	1319	36	107.4	52	8.72
5	13,876	21	1128	37	91.76	53	7.56
6	11,867	22	964.1	38	78.18	54	6.39
7	10,143	23	824.0	39	67.15	55	5.23
8	8674	24	704.3	40	57.45	56	4.64
9	7415	25	601.8	41	49.00	57	4.06
10	6336	26	514.8	42	41.81	58	3.48
11	5416	27	439.4	43	35.84	59	2.90
12	4630	28	375.9	44	30.49	60	2.32
13	3956	29	321.5	45	26.34	61	1.74
14	3383	30	274.8	46	22.21	62	1.16
15	2890	31	235.0	47	19.26	63	0.58
16	2471	32	200.9	48	16.33		

the photoelectrons dominate and the spacecraft becomes positively charged causing the measured electron population to be accelerated to greater energies as they fall through the resulting potential. In the absence of sunlight or in regions of high plasma density the potential becomes negative, due to the ambient energetic electron influx, and so the electrons will decelerate to lower energies. Before the density and temperature values can be calculated, the photoelectron population must be removed from the electron distribution and the electron counts must be corrected for their altered energies. This procedure was first described in application to the CAPS–ELS data by Rymer (2004) and correct assignment of this value is one of the biggest challenges in the analysis of the data from CAPS–ELS. A general discussion of this method is given by Johnstone et al. (1997). Fig. 3a shows a colour coded, energy–time spectrogram of the electron counts measured on anode 5 from the 30 June 2004, which corresponds to the SOI. The figure shows a population of electrons below approximately 10 eV between 00:00–1800 UT. The upper energy of this population gradually decreases until 18:00 UT when it disappears. The presence and behaviour of this population is indicative of photoelectrons being stripped from the spacecraft body by solar UV radiation and being collected by the spectrometer. The fact that photoelectrons are being stripped from the spacecraft and the return current is not large enough to redress the balance, results in the spacecraft floating at a positive potential, and so the ambient electrons will be accelerated to higher energies on entering the CAPS–ELS sensor. The top left panel of Fig. 3b is a counts-energy line plot extracted from Fig. 3a along the vertical dashed line at 12:30 UT. At that time the spacecraft was in the dayside plasma sheet. The photoelectron population can be seen on the left and the ambient electrons on the right with the two populations being separated by a dip, marked with a dashed line. This indicates the spacecraft potential,

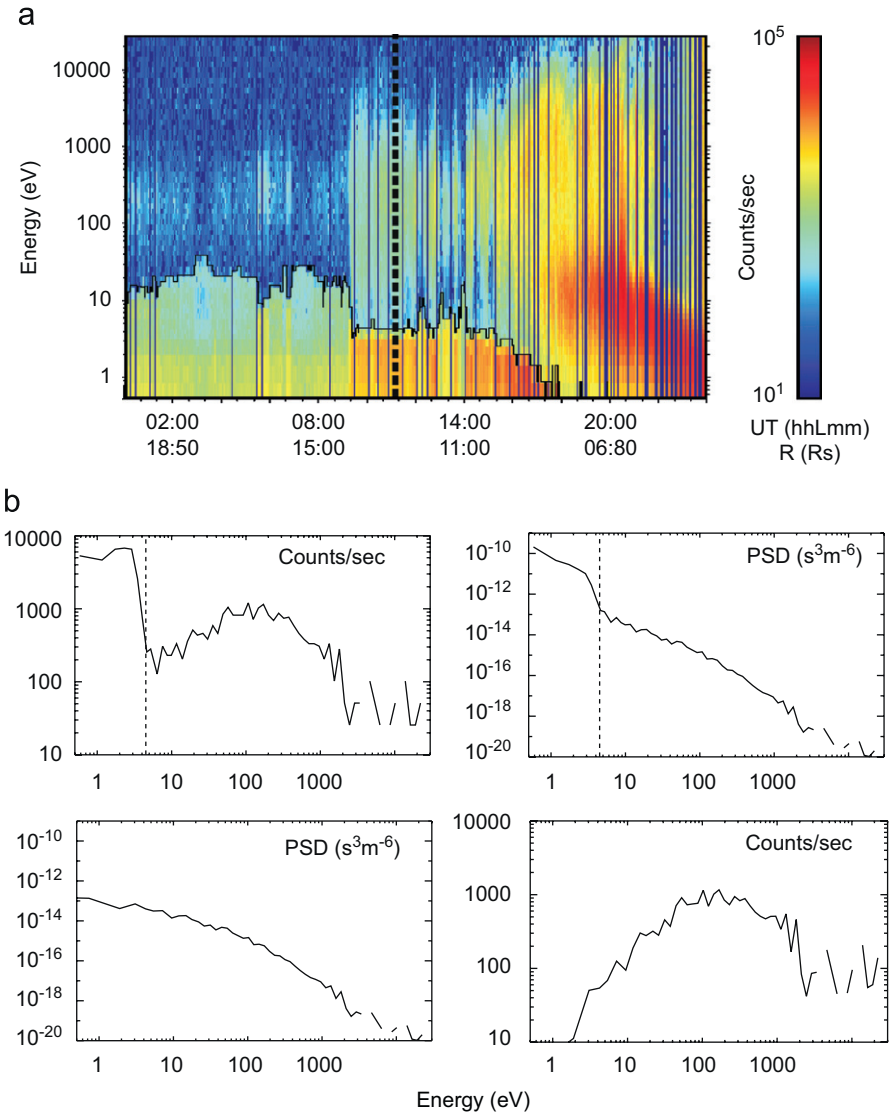

Fig. 3. An illustration of the photoelectron removal process. Fig. (a) is a 24 h, colour-coded, energy-time spectrogram on the 30 June 2004. It has energy in eV on the *y*-axis with the colour bar at the right denoting the electron counts. The *x*-axis shows time in UT hours. A black line has been drawn across the spectrogram from 10 eV on the left to 0.5 eV at 18:00 UT. This line represents the spacecraft potential derived from the dip between the photoelectron and ambient electron populations, as illustrated in the first panel of the lower image. The vertical dashed line represents the location, 12:30 UT, that the lower image panels are extracted from. The lower image shows four panels. The first, (top left) has the original data with a potential value of 4.45 eV denoted by the dashed line. The data is then converted to phase space density shown in the second panel (top right). The data is shifted to the left by the potential as shown in third panel (bottom left). The last panel (bottom right) shows the shifted and corrected data converted back to counts.

which can be used to give a measure of the electric potential that the spacecraft is floating at (Johnstone et al., 1987). The electron counts can be converted to phase space density using Eq. (1).

$$f(v) = \frac{2N}{t_a v^4 G(E)}, \tag{1}$$

where N is the returned electron count, t_a is the accumulation time minus the dead time correction (23.40 ms), v is the velocity associated with the measurement energy derived from $v = \sqrt{2E/m}$, and $G(E)$ is the instrument energy-dependent geometric factor as detailed in Linder et al. (1998). The general properties of the energy dependent geometric factor as applied to electrostatic analyzers is described in Kessel et al. (1989). The geometric factor for each anode is shown in Fig. 4. The phase space density is shown in the second panel (top right) of Fig. 3b, which has a functional dependence on the energy. Then with knowledge of the spacecraft potential, the accelerated, incident electron energies can be corrected by shifting the phase space density values along the energy scale by an amount equal to the potential in accordance with Liouville's theorem. This results in the third panel (bottom left) of Fig. 3b. Finally, the corrected phase space density values are converted back to counts and are shown in the last panel (bottom right) of Fig. 3b. This correction is limited to the case of a positive spacecraft potential. The case of negative spacecraft potential is beyond the scope of

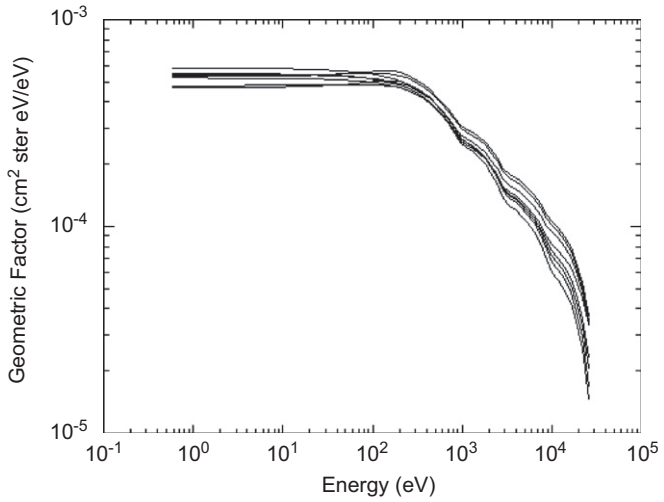

Fig. 4. The geometric factors for the eight anodes of the CAPS–ELS as a function of energy.

the present paper and requires a dedicated study in a future paper involving data sets from other instruments.

3. The 3d moment method

The traditional method of computing the bulk parameters of a space plasma is well documented in many textbooks and papers, e.g. (Baumjohann and Treumann, 1999; Boyd and Sanderson, 1969). The premise of this method is to integrate a distribution function about a volume of velocity space, the basic equation of this method being:

$$\mathbf{M_r}(\mathbf{x},t)=\int \mathbf{v}^r f(\mathbf{v},\mathbf{x},t)\,\mathrm{d}^3\mathbf{v}. \tag{2}$$

This leads to the first few moments, $r=0,1,2$, which correspond to density n, bulk flow velocity $\mathbf{v_b}$ and the stress tensor which, in the plasma rest frame is equal to the pressure tensor $\mathbf{P}$ of the distribution, respectively. The particular equations for these moments are as follows:

$$n=\int f(\mathbf{v})\,\mathrm{d}^3\mathbf{v}, \tag{3}$$

$$\mathbf{v_b}=\frac{1}{n}\int \mathbf{v} f(\mathbf{v})\,\mathrm{d}^3\mathbf{v}, \tag{4}$$

$$\mathbf{P}=m\int (\mathbf{v}-\mathbf{v_b})\cdot(\mathbf{v}-\mathbf{v_b}) f(\mathbf{v})\,\mathrm{d}^3\mathbf{v}. \tag{5}$$

The $\mathbf{v}^r$ in Eq. (2) produces an r-fold dyadic product in Eq. (5), resulting in a tensor of rank r, and so the pressure moment will be a nine-element tensor, containing a trace, diagonal part and a traceless, off-diagonal part. Only the three-diagonal terms are considered here, due to the limited spatial coverage of the instrument, assuming that the others are negligible. From the definition of the pressure tensor, we can define the temperature as follows:

$$\mathbf{T}=\frac{m}{k_\mathrm{B}n}\int (\mathbf{v}-\mathbf{v_b})\cdot(\mathbf{v}-\mathbf{v_b}) f(\mathbf{v})\,\mathrm{d}^3\mathbf{v}, \tag{6}$$

where k_B is the Boltzmann constant. If the distribution function $f(\mathbf{v})$ is known, then an analytical solution can be found. In practice, the analytical form of $f(\mathbf{v})$ is unknown. The raw data consists of electron counts at particular points in velocity space. The counts can be converted to a more physical parameter, the phase space density, using Eq. (1) with units of $\mathrm{m}^{-6}\,\mathrm{s}^3$. With the limited energy resolution of the instrument, we now re-write the above equations in a summation form over finite velocity-space elements related to the energy bin boundaries ($E\pm\Delta E/2$) of the instrument. We express the elementary volume of velocity space in spherical polar coordinates and further assume spherical symmetry due to the limited field of view of the instrument. Thus, the plasma density and scalar temperature are given by

$$n=\frac{4\pi}{3}\sum_{i=1}^{i=63}\int_{v_{i-1}}^{v_i} f(\mathbf{v})v^2\,\mathrm{d}v, \tag{7}$$

$$T=\frac{4\pi m}{3k_\mathrm{B}n}\sum_{i=1}^{i=63}\int_{v_{i-1}}^{v_i} f(\mathbf{v})v^4\,\mathrm{d}v, \tag{8}$$

where Eq. (4) is assumed to be equal to zero and the scalar temperature is derived from the trace of the temperature tensor. In these equations, $\int_{v_{i-1}}^{v_i}$ represents the integration over the width of the ith energy channel corrected from the spacecraft potential. Under the assumption that the distribution function is uniform over the width of each energy channel, Eqs. (7) and (8) can be approximated by

$$n=\frac{4\pi}{3}\sum_{i=1}^{i=63} f(v_{i,m})(v_i^3-v_{i-1}^3) \tag{9}$$

and

$$T=\frac{4\pi m}{15k_\mathrm{B}n}\sum_{i=1}^{i=63} f(v_{i,m})(v_i^5-v_{i-1}^5), \tag{10}$$

where $v_{i,m}$ is related to the mid-energy of the ith channel. The resulting equations have been used in the past to determine plasma parameters from various missions (e.g., AMPTE-UKS Kessel et al., 1989; LANL-MPA Thomsen et al., 1999; Cluster-PEACE, *A. Fazakerley*, private communication). CAPS–ELS plasma parameters obtained with our 3d method have been used so far in all published articles that include low-energy electron observations. During the analysis, Eqs. (9) and (10) are used to return a set of scalar values for the electron density and temperature, respectively. However, the arrays of values prior to the final summation are also saved. The density and temperature can then be summed over a selected energy range. This is useful when multiple populations of electrons are present in which case, Eq. (10) will provide an average value of the electron temperature. For example, if two populations are present (a cold one denoted by subscript c, and a hot one, denoted by subscript h), the density and temperature

values will be given by

$$n = n_c + n_h, \tag{11}$$

$$T = \frac{n_c T_c + n_h T_h}{n_c + n_h}. \tag{12}$$

4. The 1d moment method

The second technique we use to estimate the electron density and temperature was first developed for CAP-S–ELS by Rymer (2004). It was designed as a quick and easy way of extracting a density and temperature value from the ELS counts data and relies on the approximation that the energy distribution function can be represented by a Maxwellian given by

$$f(E) = n\left(\frac{m}{2\pi k_B T}\right)^{3/2} \exp\left(\frac{-E}{k_B T}\right). \tag{13}$$

By inserting this expression into Eq. (1) and differentiating with respect to energy, the count rate $R_c = N/t_a$, can be written as

$$\frac{dR_c}{dE} = CGE \exp\left(\frac{-E}{k_B T}\right)\left(2 - \frac{E}{k_B T} + \frac{d\ \ln(G)}{d\ \ln(E)}\right), \tag{14}$$

where $C = 2n/\sqrt{(m)}(1/2\pi k_B T)^{3/2}$. We then obtain the electron temperature by looking for the energy E_p that maximizes the count rate. To find this energy, we use a Gaussian fitting routine of the form:

$$f(x) = A_0 \exp\left(\left(\frac{x - A_1}{A_2}\right)^2 \Big/ 2\right). \tag{15}$$

This routine returns A_0, A_1, A_2 which are the, height, centre and width of the Gaussian, respectively. An example of a Gaussian curve fitted to the data is shown in Fig. 5. At the peak of the Gaussian, $E = E_p$ and so $dR_c/dE = 0$. This enables us to write the following expression for temperature:

$$E_p = k_B T\left(2 + \frac{d\ \ln(G)}{d\ \ln(E)}\right) \Rightarrow T = \frac{E_p}{k_B\left(2 + \frac{d\ \ln(G)}{d\ \ln(E)}\right)}. \tag{16}$$

We neglect the second factor of the denominator of Eq. (16) which, allows us to write the following expression for temperature.

$$T = \frac{E_p}{2k_B}. \tag{17}$$

By neglecting the differential term from Eq. (16) we introduce a minimal uncertainty in the region 0–200 eV and an error of 23% in the region 200–11 000 eV. This error is acceptable in view of the associated errors with the instrument's energy resolution. By estimating the count rate at this energy, R_{cp}, we can obtain the electron density with

$$n = \frac{\pi^{3/2}}{2^{3/2} G} R_{cp} \sqrt{\frac{m}{k_B T}} \exp(2), \tag{18}$$

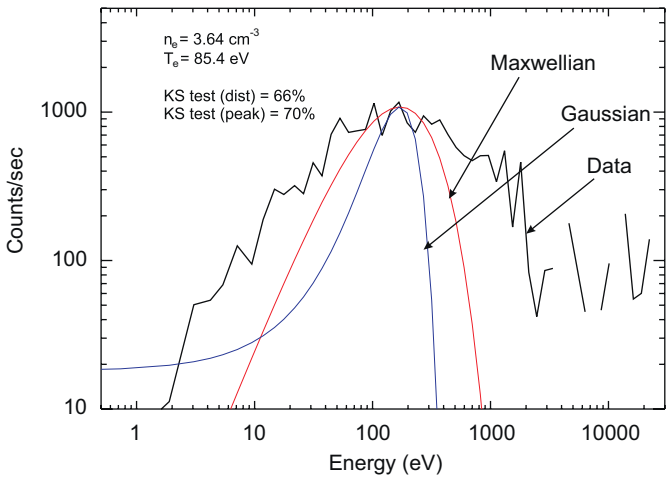

Fig. 5. An example of the fitting technique used in the 1d method. The black line is the counts per second data from the CAPS–ELS having been corrected for photoelectrons. A Gaussian curve is fitted shown in blue. Using the density and temperature values derived from the peak of this curve, a Maxwellian is derived using Eq. (13). The Maxwellian shown in red is used to perform two KS tests against the ELS counts data. The results of these tests are shown on the plot.

where R_{cp} is the count rate at the distribution peak. Once the density and temperature values have been determined, a Maxwellian is derived using Eq. (13) and a Kolmogorov–Smirnoff goodness of fit test is performed between the entire distribution and the derived Maxwellian curve. This test is also performed on five points surrounding the peak of the fitted curve. Fig. 5 shows an example of the derived Maxwellian curve fitted to the original data. The results of the KS tests show that the derived Maxwellian has a 70% confidence. The KS test results are saved with 1d technique values so that the user can filter the density and temperature values on the basis of the KS results. This method can also be used to study multiple populations by restricting the energy range in which the energy peak occurs, so that a density and temperature value for a cold or a hot population can be returned. To maximize the accuracy of this technique, the fitted Maxwellian curve can be removed from the velocity distribution and a second Maxwellian fitted to the remainder. This process can be done n times returning n density and temperature values depending on the number of populations present. One advantage of this method is the ability to apply the "goodness-of-fit" criterion described above, which can be used to filter out errors caused by poorly assigned spacecraft potentials. Another advantage is that it can be easily applied to other analytical representations of velocity distributions, such as kappa distributions (Vasyliunas, 1968). These distributions have been used to represent observed distributions with a high-energy tail. This however is beyond the scope of this present paper. This method will not be used as the main supplier of ELS moments to the planetary data system (PDS). It is used solely as a 'rough and ready' technique, and is employed here as a cross check for the 3d technique.

Previous published studies have however used the outputs of this method (Rymer, 2004; Sittler et al., 2005; Young et al., 2005).

5. Application and comparison of the 1d and 3d methods

In this section we apply the 1d and 3d methods to derive electron fluid parameters from CAPS–ELS measurements obtained during SOI on June 30th and July 1st 2004 (day of year (DOY) 182 and 183). We shall use the observed, large-scale structure of the saturnian magnetosphere to compare and discuss the derived electron densities and temperatures in the corresponding magnetospheric regions.

5.1. Plasma populations and boundaries

During SOI, the Cassini spacecraft was embedded in the Saturnian magnetosphere and stayed below the Saturnian equatorial plane, except for briefly before and after closest approach, when it crossed this plane twice at around $2.6R_s$. There were no targetted encounters with any of the Saturnian satellites, apart from the unique pass through the ring system of the planet. Cassini's closest approach distance was 1.33 Saturn Radii (R_s), at 02:40 UT on July 1st 2004 (DOY 183). Based on measurements taken by the CAPS instruments 24 h either side of closest approach, Young et al. (2005) has provided an initial overview of Saturn's magnetospheric plasma populations and the boundaries between them. This has been followed by a more comprehensive description by André et al. (2007), based on the full data set from the Magnetospheric and Plasma instruments on board Cassini. Observations of large-scale changes in the bulk properties and composition of the low-energy electron and ion plasma have enabled us to distinguish, both on the inbound and the outbound pass, four distinct regions in Saturn's magnetosphere (André et al., 2007). Using observations from the CAPS–ELS spectrometer the properties of electron populations in these regions can be summarized as follows. Beginning with the outermost regions and moving inwards, the Cassini spacecraft encountered; Region 1: The high-latitude magnetosphere. Here the low-energy plasma is almost absent since Cassini is located well below the equatorial plane where the plasma is more concentrated by the centrifugal force arising from Saturn's fast rotation. Region 2: The dynamic and extended plasma sheet. This is located inside $14.4R_s$ inbound and $13.6R_s$ outbound. In this region the plasma contains two electron populations, a cold (a few tens of eV) and a hot (a few hundreds of eV) populations, likely to be the result of plasma transport processes (Hill et al., 2005; Burch et al., 2005; Rymer et al., 2007). Region 3: The cold plasma and neutral torus. Located inside $6R_s$ inbound and outbound, this region is dominated by cold electrons (a few eV) and devoid of hot electrons, whose sink may be related to the vast amount of neutral gas observed in this region (Esposito et al., 2005). This region also contains the radiation belt region, where very energetic (>1 MeV) electrons are present. These electrons, however, are beyond the energy range of our instrument. Region 4: The ring ionosphere. Within $3R_s$ inbound and outbound, Cassini encounterd the ring's ionosphere where the fluxes of the low-energy electrons seen on the shaded side of the rings are directly anti-correlated with their optical thickness (Coates et al., 2005). At the end of DOY 182, from ~24: 00 to ~05: 00 UT DOY 183, penetrating radiation contaminated the CAPS–ELS sensor and polluted the observations of the low-energy plasma. The boundaries of these different regions are delineated by vertical lines on the energy-time spectrogram represented in Fig. 6a except for region 4.

5.2. CAPS–ELS moments: 1d versus 3d results

Fig. 6 shows the results of the 1d and 3d moments (densities in panel c, and temperatures in panel d) in addition to the energy-time spectrogram (panel a) represented in Fig. 6a. Initially, only one plasma population is considered in the 1d method. Photoelectrons are observed all along the trajectory until 18:00 UT DOY 182, when they disappear and reappear again at 11:00 UT DOY 183. This indicates that the spacecraft surface became negatively charged in the deepest regions of the magnetosphere. The spacecraft potential used in the derivation of the electron parameters is given by the maximum energy of the observed photoelectrons and is taken to be zero when not constrained by the data (i.e., when negative). This leads to an underestimation of the density in these regions, as well as a significant drop in the temperature of the low-energy electron populations. The outputs of our 1d method have nevertheless been used by Sittler et al. (2005) to analyse Saturn's inner plasmasphere during the time interval 18:00–24:00 on DOY 182. Electron temperature of a few eV were reported for the first time inside of Enceladus' orbit. Such cold electron populations were not detected by the Voyager plasma instrument that had a low-energy cutoff of 10 eV. The overall results show that there are discrepancies in the densities derived from the two methods. The values in region 1 show good agreement, however, except in some isolated instances in region 2 where the two methods show some agreement, the 1d values are generally below the 3d values by approximately 60%. Although not as pronounced, the difference continues into region 3. In the case of the temperatures, there are short periods where the 1d temperature deviates from its norm and becomes higher than that of the 3d. However, the results show that the 3d method gives generally higher density than the 1d method, regardless of the regions. This is to be expected as the 1d method only accounts for the electron population described by the Maxwellian curve, whereas the 3d method takes into account the entire electron distribution. The two methods should give good agreement where there is a clear and distinct electron population with a clearly dominant Maxwellian component. This is observed to be the case in region 2, and we do indeed observe the two methods to be in good agreement in

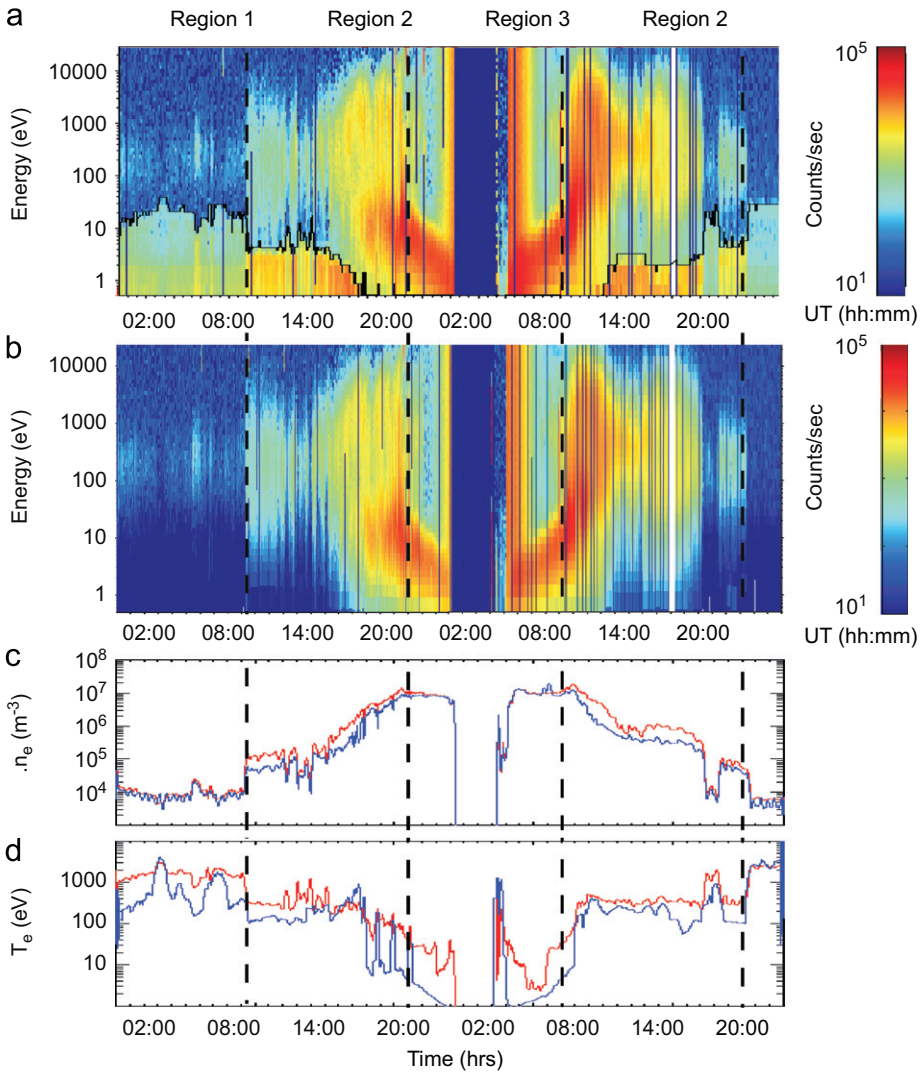

Fig. 6. Panel a shows a 48 h, colour-coded, energy-time spectrogram from the 0:00 UT 30 June 2004 to 24:00 UT 01 July 2004. It has energy in eV on the *y*-axis with the colour bar at the right denoting the electron counts. The *x*-axis shows time in UT hours. A black line has been drawn across the spectrogram from ~10 eV on the left to ~20 eV on the right. This line marks the upper boundary of the photoelectrons and represents the spacecraft potential. At ~18: 00 UT (DOY 182) the potential becomes negative and returns positive at ~11: 00 UT (DOY 183). Vertical dashed lines have been drawn at 09:30 and 21:00 UT (DOY 182) and 08:00 and 21:00 UT (DOY 183) to show the locations of the boundaries between different regions of the magnetosphere. Panel (b) shows the spectrogram from panel a with the photoelectrons removed. Panels (c) and (d) show the corresponding derived densities and temperatures respectively. The 3d method is shown in red and the 1d method is shown in blue. The vertical dashed lines show the boundaries between the regions outlined above. The derived values in the regions where the data has been contaminated by background radiation have been removed.

that region. In the presence of several electron populations, the 1d method, restricted to only one population will underestimate the electron density when compared with the 3d method, as shown in Fig. 6. We can achieve better agreement in all regions of the magnetosphere by considering two electron populations (a cold one, below 100 eV, and a hot one, above 100 eV) as in Young et al. (2005). We derive the corresponding densities and temperatures, by summing over selected energy ranges in the 3d method and by applying the 1d method separately to the observed hot and cold populations. Fig. 7 shows the densities and temperatures of the hot and cold population calculated using the 3d method (red) and the 1d method (blue). Clearly there is an overall improvement in the comparison between the two methods mainly in the densities (temperatures should still be considered with more caution). In regions 2 and 3 the comparison is greatly improved when two populations are taken into account emphasizing the fact that there are two populations present and that they must be treated separately in order to calculate the density and temperature values correctly. In region 1 the comparison between the two methods gives satisfactory results as far as the hot population is concerned. The cold population comparison is not so good, however neither hot or cold is as good as the single population comparison for region 1 as shown in Fig. 6. Thus implying that when there is a single population present, both methods work well.

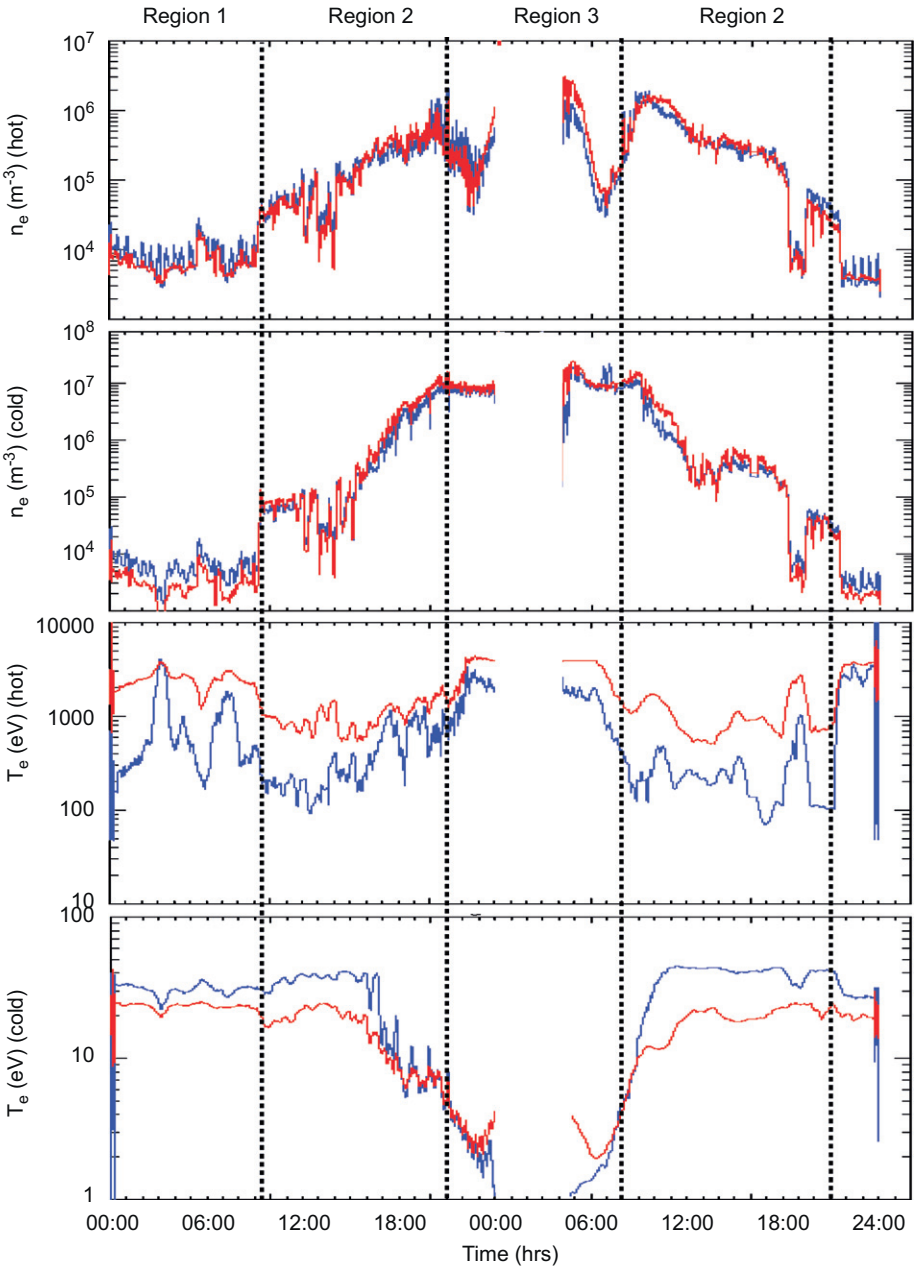

Fig. 7. The derived density and temperature of the hot and cold electron populations calculated from the 1d method shown in blue and the 3d method shown in red. The upper panel shows the electron density results for the hot population. The second panel shows the electron density results for the cold population. The third panel shows the electron temperature of the hot population, and finally the last panel shows the electron temperature of the cold population.

5.3. Discussion

Having illustrated how the two methods give similar results when two electron populations are taken into account, we use the derived parameters to estimate the partitioning of electron density and pressure between cold and hot electrons. The pressure is obtained from $P = nkT$. Fig. 8 displays the ratios of hot electron densities and pressures divided by the total CAPS–ELS density and pressure using the results of the 3d method. The total electron pressure is also shown. This replicates an earlier study by Sittler et al. (1983), using observations from the Voyager Plasma Spectrometer (PLS, energy range 10 eV to 6 keV). The partitioning results in Fig. 8 demonstrate that in region 1 where the plasma has energies approaching 1 keV, the hot electrons dominate. Occupying approximately 70% of the total density and almost all of the total pressure. A sudden decrease in the density values at $L = 14.4R_s$ inbound, marks the outer boundary of region 2. As the cold electron population becomes more abundant in this region, we see the hot electron density decrease suddenly to 30%, then recover to approximately 50% throughout the region. The total pressure in region 2 remains dominated by the hot electron contribution.

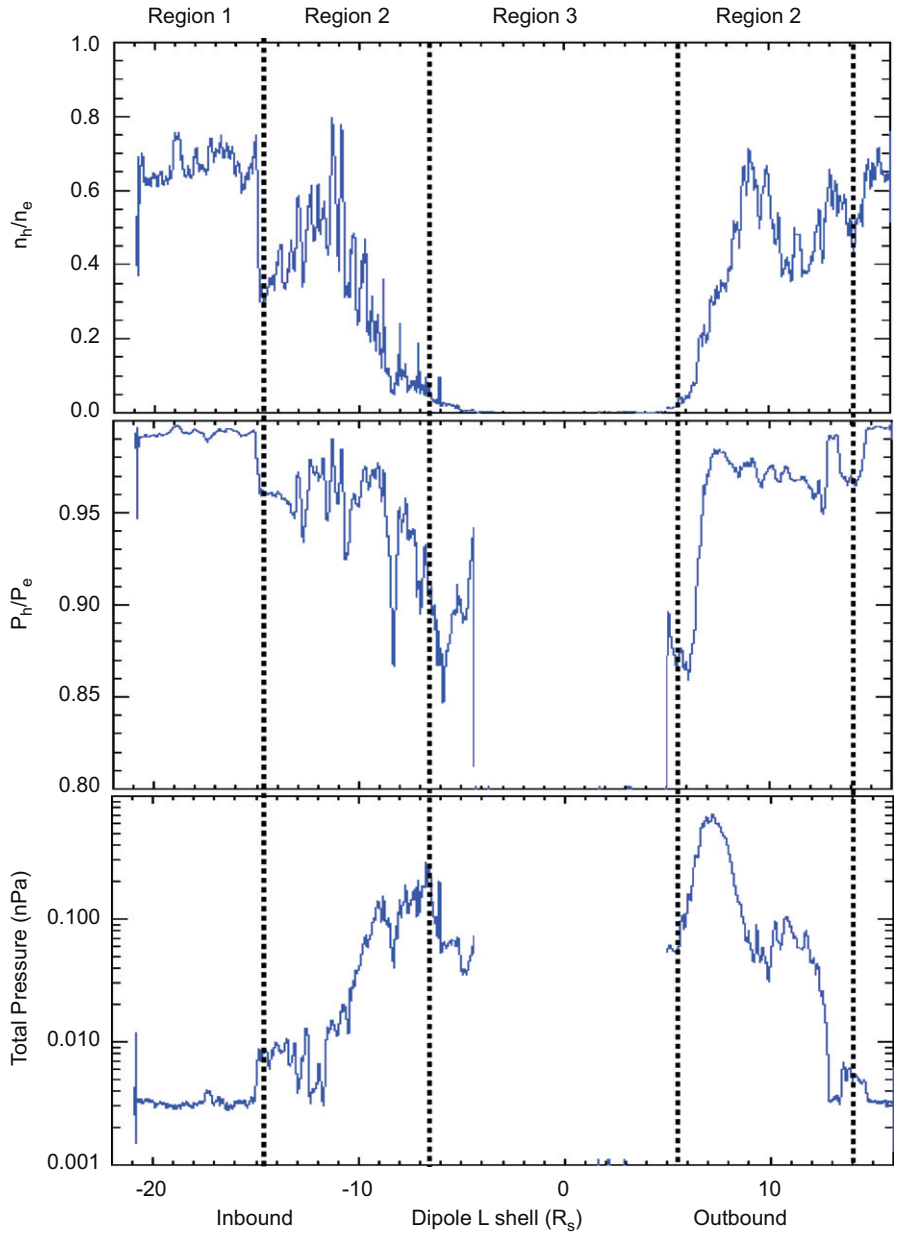

Fig. 8. From top to bottom: (a) Ratio of (hot electron density/total density). (b) Ratio of (hot electron pressure/total pressure). (c) Total electron pressure.

As Cassini passes into region 3, the cold inner magnetosphere, we see the density of the hot electrons diminishes considerably and the cold electrons becoming the dominant contributor. As in region 1 and 2, the total pressure in region 3 is again dominated by the hot electrons. After $L = 5R_s$ inbound, the data is contaminated by background radiation and negative spacecraft potential effects and becomes unreliable. Throughout the entire outbound pass, we see the hot electron population dominating the pressure in all regions. The total density is dominated by the cold electrons in region 3, with the hot electrons becoming gradually significant in region 2. The importance of the hot and cold electrons to the overall density fluctuates throughout this region between 40% and 60%. Then, similarly to the inbound observations, a sharp increase in the hot population density is observed thus marking the outer boundary of region 2. Such a study will need to be complemented by combining the electron energy spectra measured by the particle instruments on board Cassini in different energy ranges and applying the 3d method to the resulting composite spectra. In particular, the low-energy magnetospheric measurement system (LEMMS) of the Magnetospheric Imaging Instrument (MIMI) (Krimigis et al., 2004), overlaps the CAPS–ELS instrument at its lower energies and the merging of these two data sets will enable us to complete the previous study by Maurice et al. (1996), based on data from the three Voyager particle instruments.

6. Conclusions

In this paper we have presented the two methods currently employed to derive electron fluid parameters from the CAPS–ELS spectrometer on board the Cassini spacecraft. We have emphasized particularly, their application to Cassini SOI observations in the saturnian environment and have compared the results with each other. These two methods use very different approaches (fitting versus integrating the measured distribution function) but give satisfactory agreement when the physical properties of the environment inferred from inspection of the raw data are carefully considered. It is therefore advisable to inspect the energy-time spectrograms in order to fully understand what is represented by the derived parameters. The use of both methods in a complementary way is recommended. At this stage of the analysis, both methods are restricted to the assumption of an isotropic electron distribution, and consequently, only a limited part of the information recorded by the CAPS–ELS spectrometer is used to derive electron moments, from measurements obtained by one single anode. Future improvements of the analysis will need to combine the measurements obtained by all anodes as well as the motion of the rotating platform in order to derive moments corresponding first to gyrotropic and then to the real electron distributions. We re-state here that the 3d method described in the text is the method used to provide electron moments to the PDS. The 1d method described in the text is used solely as a cross reference for the 3d method. Measurements in regions where the spacecraft potential appears negative, and hence where the low energy part of the electron spectrum is hidden from observation, will require a more thorough analysis in the future. In these regions, the two methods can only give approximate results and lead to an underestimate of the electron density. Based on a survey of most orbits available to date, negative spacecraft potentials are observed systematically in the inner saturnian magnetosphere (inside of $8R_s$) as well as in the vicinity of Titan's ionosphere. Future improvements of the analysis will make use of additional observations from other magnetosphere and plasma instruments on board Cassini in order to account for negative spacecraft potential correction in the derivation of electron moments. Several possibilities have already been identified and are currently being investigated, in order to estimate the spacecraft potential and reconstruct the hidden part of the electron spectrum, based on the combination of the following data sets: CAPS–ELS and radio and plasma wave science data (RPWS) Gurnett et al. (2004): The RPWS total electron density determined from upper hybrid resonance emissions (Gurnett et al., 2005; Persoon et al., 2005) or from quasi-thermal noise spectroscopy (Moncuquet et al., 2005) can be used to infer the spacecraft potential correction (Sittler et al., 1983) required for CAPS–ELS densities to match RPWS densities. This method has been used in Tokar et al. (2006) with CAPS–IMS ion parameters as the input; CAPS–ELS, CAPS–IMS and CAPS-IBS data: When the spacecraft becomes negatively charged, the measured ion populations will be accelerated. An estimate of this acceleration can be used as a proxy for the spacecraft potential; CAPS–ELS and Langmuir Probe data (LP) (Wahlund et al., 2005): The spacecraft potential measured by the LP can be used as a direct input. The LP instrument however is located on a different part of the spacecraft, and on a 1m boom and so this method can have limitations. Finally, let us point out that the methods developed to derive electron densities and temperatures from the Cassini–Huygens CAPS electron spectrometer are similar to the ones developed for the analysis of the data returned by the ASPERA-3 instrument on board Mars Express (Fraenz et al., 2006), as well as by the ASPERA-4 instrument on board Venus-Express. All these instruments are mounted on three-axis stabilized spacecraft and are constrained by their limited field of view, which slightly complicates the analysis of the returned plasma data compared to instruments mounted on spinning spacecrafts.

References

André, N., Blanc, M., Maurice, S., Schippers, P., Pallier, E., Gombosi, T., Hansen, K., Young, D., Crary, F., Bolton, S., Sittler, E., Smith, H., Johnson, R., Baragiola, R., Coates, A., Rymer, A., Dougherty, M., Achilleos, N., Arridge, C., Krimigis, S., Mitchell, D., Krupp, N., Hamilton, D., Dandouras, I., Gurnett, D., Kurth, W., Louran, P., Srama, R., Kempf, S., Waite, H., Clarke, J., Esposito, L., 2007. Cassini Saturn Orbit Insertion observations reveal a multi-faceted magnetosphere at Saturn. Geophys., submitted for publication.

Baumjohann, W., Treumann, R.A., 1999. Basic Space Plasma Physics. Imperial College Press.

Blanc, M., Bolton, S., Bradley, J., Burton, M., Cravens, T.E., Dandouras, I., Dougherty, M.K., Festou, M.C., Feynman, J., Johnson, R.E., Gombosi, T.G., Kurth, W.S., Liewer, P.C., Mauk, B.H., Maurice, S., Mitchell, D., Neubauer, F.M., Richardson, J.D., Shemansky, D.E., Sittler, E.C., Tsurutani, B.T., Zarka, P., Esposito, L.W., Grün, E., Gurnett, D.A., Kilore, A.J., Krimigis, S.M., Southwood, D., Waite, J.H., Young, D.T., 2002. Magnetospheric and Plasma Science with Cassini–Huygens. Space Sci. Rev. 104, 253–346.

Boyd, T.J.M., Sanderson, J.J., 1969. Plasma Dynamics. Thomas Nelson and Sons Ltd.

Burch, J.L., Goldstein, J., Hill, T.W., Young, D.T., Crary, F.J., Coates, A.J., André, N., Kurth Jr., E.E.S., 2005. Properties of local plasma injections in Saturn's Magnetosphere. Geophys. Res. Lett. 32, L14S02.

Coates, A.J., Alsop, C., Coker, A.J., Linder, D.R., Johnstone, A.J., Woodliffe, R.D., Grande, M., Preece, A., Burge, S., Hall, D.S., 1996. The electron spectrometer for the cassini spacecraft. J. British Interplanetary Soc. 45 (9).

Coates, A.J., McAndrews, H.J., Rymer, A.M., Young, D.T., Crary, F.J., Maurice, S., Johnson, R.E., Baragiola, R.A., Tokar, R.L., Sittler, E.C., Lewis, G.R., 2005. Plasma electrons above Saturn's main rings: CAPS observation. Geophys. Res. Lett. 32, L14S09.

Esposito, L.W., Colwell, J.E., Larsen, K., McClintock, W.E., Stewart, A.I.F., Hallett, J.J.T., Shemansky, D.E., Ajello, J.M., Hansen, C.J., Hendrix, A.R., West, R.A., Keller, H.U., Korth, A., Pryor, W.R., Reulke, R., Yung, Y.L., 2005. Ultraviolet imaging spectroscopy shows an active Saturnian system. Science 307, 1251–1255.

Fraenz, M., Dubinin, E., Roussos, E., Woch, J., Winningham, J.D., Frahm, R., Fedorov, A., Coates, A.J., Barabash, S., Lundin, R., 2006. Plasma moments in the environment of Mars. Space Sci. Rev. 126, 165–207.

Gurnett, D.A., Kurth, W.S., Kirchner, D.L., Hospodarsky, G.B., Averkamp, T.F., Zarka, P., Lecacheux, A., Manning, R., Roux, A., Canu, P., Cornilleau-Wehrlin, N., Galopeau, P., Meyer, A., Boström, R., Gustafsson, G., Wahlund, J.E., Ahlen, L., Rucker, H.O., Ladreiter, H.P., Macher, W., Woolliscroft, L.J.C., Alleyne, H., Kaiser, M.L., Desch, M.D., Farrell, W.M., Harvey, C.C., Louarn, P., Kellogg, P.J., Goetz, K., Pedersen, A., 2004. The Cassini radio and plasma wave investigation. Space Sci. Rev. 114, 395–463.

Gurnett, D.A., Kurth, W.S., Hospodarsky, G.B., Persoon, A.M., Averkamp, T.F., Cecconi, B., Lecacheux, A., Zarka, P., Canu, P., Cornilleau-Wehrlin, N., Galopeau, P., Roux, A., Harvey, C., Louarn, P., Bostrom, R., Gustafsson, G., Wahlund, J.E., Desch, M.D., Farrell, W.M., Kaiser, M.L., Goetz, K., Kellogg, P.J., Fischer, G., Ladreiter, H.P., Rucker, H., Alleyne, H., Pedersen, A., 2005. Radio and Plasma Wave observations at Saturn from Cassini's approach and first orbit. Science 307, 1255–1259.

Hill, T.W., Rymer, A.M., Burch, J.L., Crary, F.J., Young, D.T., Thomsen, M.F., Delapp, D., André, N., Coates, A.J., Lewis, G.R., 2005. Evidence for rotationally driven plasma transport in Saturn's Magnetosphere. Geophys. Res. Lett. 32, L14S10.

Johnstone, A.D., Coates, A.J., Wilken, B., Studemann, W., Weiss, W., Cerulli-Irelli, R., Formisano, V., Borg, H., Olsen, S., Winningham, J.D., Bryant, D.A., Kellock, S.J., 1987. The Giotto three-dimensional positive analyser. J. Phys. E: Sci. Instrum. 20, 795–802.

Johnstone, A.D., Alsop, C., Burge, S., Carter, P.J., Coates, A.J., Coker, A.J., Fazakerley, A.N., Grande, M., Gowen, R.A., Gurgiolo, C., Hancock, B.K., Narheim, B., Preece, A., Sheather, P.H., Winningham, J.D., Woodliffe, R.D., 1997. Peace: A plasma electron and current experiment. Space Sci. Rev. 79, 351–398.

Kessel, R.L., Johnstone, A.D., Coates, A.J., Gowen, R.A., 1989. Space plasma measurements with ion instruments. Rev. Sci. Instrum. 60, 3750–3761.

Krimigis, S.M., Mitchell, D.G., Hamilton, D.C., Livi, S., Dandouras, J., Jaskulek, S., Armstrong, T.P., Boldt, J.D., Cheng, A.F., Gloeckler, G., Hayes, J.R., Hsieh, K.C., Ip, W.-H., Keath, E.P., Kirsch, E., Krupp, N., Lanzerotti, L.J., Lundgren, R., Mauk, B.H., McEntire, R.W., Roelof, E.C., Schlemm, C.E., Tossman, B.E., Wilken, B., Williams, D.J., 2004. Magnetosphere Imaging Instrument (MIMI) on the Cassini mission to Saturn/Titan. Space Sci. Rev. 114, 233–329.

Linder, D.R., Coates, A.J., Woodliffe, R.D., Alsop, C., Johnstone, A.D., Grande, M., Preece, A., Narheim, B., Young, D.T., 1998. The Cassini CAPS Electron Spectrometer, Measurement Techniques in Space Plasmas: Particles Geophysical Monograph, vol. 102, American Geophysical Union, pp. 257–262.

Maurice, S., Sittler, E.C., Cooper, J.F., Mauk, B.H., Blanc, M., Selesnick, R.S., 1996. Comprehensive analysis of electron observations at saturn: Voyager 1 and 2. J. Geophys. Res. 101, 15221–15232.

Moncuquet, M., Lecacheux, A., Meyer-Vernet, N., Cecconi, B., Kurth, W.S., 2005. Quasi-thermal noise spectroscopy in the inner magnetosphere of Saturn with Cassini/RPWS: Electron temperature and density. Geophys. Res. Lett. 32, L20S02.

Paschmann, G., Fazakerley, A.N., Schwartz, S.J., 1998. Moments of Plasma Velocity Distributions. ISSI Scientific Report SR-001. pp. 125–158 (Chapter 6).

Persoon, A.M., Gurnett, D.A., Kurth, W.S., Hospodarsky, G.B., Groene, J.B., Canu, P., Dougherty, M.K., 2005. Equatorial electron density measurements in Saturn's inner magnetosphere. Geophys. Res. Lett. 32, 23105.

Rymer, A.M., 2004. Analysis of Cassini plasma and magnetic field measurements from 1–7 AU. Ph.D. Thesis, University College London, UK.

Rymer, A.M., Mauk, B.H., Hill, T.W., Paranicas, C., André, N., Sittler, E.C., Mitchell, D.G., Smith, H.T., Johnson, R.E., Coates, A.J., Young, D.T., Bolton, S.J., Thomsen, M.F., Dougherty, M.K., 2007. Electron sources in Saturn's magnetosphere. J. Geophys. Res. 112, A02201.

Sittler, E.C., Ogilvie, K.W., Scudder, J.D., 1983. Survey of Low-Energy Plasma Electrons in Saturn's Magnetosphere: Voyagers 1 and 2. J. Geophys. Res. 88, 8847–8870.

Sittler, E.C., Thomsen, M., Chornay, D., Shappirio, M.D., Simpson, D., Johnson, R.E., Smith, H.T., Coates, A.J., Rymer, A.M., Crary, F., McComas, D.J., Young, D.T., Reisenfeld, D., Dougherty, M., Andre, N., 2005. Preliminary results on Saturn's inner plasmasphere as observed by Cassini: Comparison with Voyager. Geophys. Res. Lett. 32, L14S07.

Thomsen, M.F., Noveroske, E., Borovsky, J.E., McComas, D.J., 1999. Calculation of moments from measurements by the Los Alamos Magnetospheric Plasma Analyzer. LA-13566-MS report.

Tokar, R.L., Johnson, R.E., Hill, T.W., Pontius, D.H., Kurth, W.S., Crary, F.J., Young, D.T., Thomsen, M.F., Reisenfeld, D.B., Coates, A.J., Lewis, G.R., Sittler, E.C., Gurnett, D.A., 2006. The interaction of the atmosphere of enceladus with saturn's plasma. Science 311, 1409–1412.

Vasyliunas, V.M., 1968. A survey of low-energy electrons in the evening sector of the magnetosphere with OGO 1 and OGO 3. J. Geophys. Res. 73, 2839.

Wahlund, J.E., Boström, R., Gustafsson, G., Gurnett, D.A., Kurth, W.S., Averkamp, T., Hospodarsky, G.B., Persoon, A.M., Canu, P., Pedersen, A., Desch, M.D., Eriksson, A.I., Gill, G., Morooka, M.W., André, M., 2005. The inner magnetosphere of Saturn: Cassini RPWS cold plasma results from the first encounter. Geophys. Res. Lett. 32, L20S09.

Whipple, E.C., 1981. Potentials of surfaces in space. Rep. Progr. Phys. 44, 1197–1250.

Young, D.T., Berthelier, J.J., Blanc, M., Burch, J.L., Coates, A.J., Goldstein, R., Grande, M., Hill, T.W., Johnson, R.E., Kelha, V., McComas, D.J., Sittler, E.C., Svenes, K.R., Szegö, K., Tanskanen, P., Ahola, K., Anderson, D., Bakshi, S., Baragiola, R.A., Barraclough, B.L., Black, R.K., Bolton, S., Booker, T., Bowman, R., Casey, P., Crary, F.J., Delapp, D., Dirks, G., Eaker, N., Funsten, H., Furman, J.D., Gosling, J.T., Hannula, H., Holmlund, C., Huomo, H., Illiano, J.M., Jensen, P., Johnson, M.A., Linder, D.R., Luntama, T., Maurice, S., McCabe, K.P., Mursula, K., Narheim, B.T., Nordholt, J.E., Preece, A., Rudzki, J., Ruitberg, A., Smith, K., Szalai, S., Thomsen, M.F., Viherkanto, K., Vilppola, J., Vollmer, T., Wahl, T.E., Wüest, M., Ylikorpi, T., Zinsmeyer, C., 2004. Cassini Plasma Spectrometer Investigation. Space Sci. Rev. 114, 395–463.

Young, D.T., Berthelier, J.J., Blanc, M., Burch, J.L., Bolton, S., Coates, A.J., Crary, F.J., Goldstein, R., Grande, M., Hill, T.W., Johnson, R.E., Baragiola, R.A., Kelha, V., McComas, D.J., Mursula, K., Sittler, E.C., Svenes, K.R., Szegö, K., Tanskanen, P., Thomsen, M.F., Bakshi, S., Barraclough, B.L., Bebesi, Z., Delapp, D., Dunlop, M.W., Gosling, J.T., Furman, J.D., Gilbert, L.K., Glenn, D., Holmlund, C., Illiano, J.M., Lewis, G.R., Linder, D.R., Maurice, S., McAndrews, H.J., Narheim, B.T., Pallier, E., Reisenfeld, D., Rymer, A.M., Smith, H.T., Tokar, R.L., Vilppola, J., Zinsmeyer, C., 2005. Composition and Dynamics of Plasma in Saturn's Magnetosphere. Science 307, 1262–1266.